Journal of Alloys and Compounds 509 (2011) 3357–3362

Contents lists available at ScienceDirect

Journal of Alloys and Compounds

journal homepage: www.elsevier.com/locate/jallcom

Solid solution strengthening in polycrystals of Mg–Sn binary alloys

B.Q. Shi [a,b], R.S. Chen [a,*], W. Ke [a]

[a] State Key laboratory for Corrosion and Protection, Institute of Metal Research, Chinese Academy of Sciences, PR China
[b] Graduate School of the Chinese Academy of Sciences, Beijing 100049, PR China

ARTICLE INFO

Article history:
Received 16 September 2010
Received in revised form 9 December 2010
Accepted 9 December 2010
Available online 16 December 2010

Keywords:
Mg–Sn alloys
Solid solution strengthening
Softening effect

ABSTRACT

Solid solution effects on the hardness and flow stress in Mg–Sn binary alloys with Sn content between 0.18% and 2.18% at temperatures ranging from ambient to 623 K were investigated in this study. At room temperature, the hardness increases with the Sn content as $H_{v0.5} = 28.3 + 6.88c$, the 0.2% proof strength (corrected for grain size strengthening effect) and c^n follow a linear relationship, where c is the solute atom fraction and $n = 1/2$ or $2/3$. The results suggest that the strengthening of basal planes controls the solid solution strengthening in polycrystals of Mg–Sn binary alloys. However, the c^n power-law is not applicable in the temperature range from 423 K to 623 K, which is proposed to be ascribed to the competition between solid solution strengthening and softening effect.

1. Introduction

Recently Mg–Sn based alloys have been given tremendous attention, and were deemed to be new cost-effective heat-resistance magnesium alloys [1–6]. The Mg–Sn system shows some characteristics in terms of creep resistance due to the formation of Mg_2Sn phase with a high melting temperature of 1043 K [1–9]. Moreover, with the aid of thermodynamic modeling for Mg–Sn based ternary system [4–6], we can better understand the relationship of the phase constituents and compositions to design new alloys.

Similar to typical binary Mg–Al, Mg–Zn and Mg–RE (RE stands for rare earth elements) phase diagrams, the Mg–Sn system is a eutectic and precipitation–hardenable system [4]. Up to now, there have been some researches on improving the precipitation strengthening by changing the state of precipitation with addition of Zn or other minor elements [2,3]. Except for precipitation strengthening, solid solution strengthening is another important strengthening mechanism in magnesium alloys. However, in contrast to Mg–Al, Mg–Zn, Mg–Y and Mg–Gd systems [10–13], the solid solution strengthening in the Mg–Sn based alloys are not clear. Additionally, little experimental work has been carried out on the concentration dependence of solid solution strengthening in polycrystals of Mg–Sn binary alloys at elevated temperatures.

In this work, the solid solution effects on the hardness and 0.2% proof strength for polycrystalline Mg–Sn binary alloys with various Sn concentrations were studied. The tensile tests were carried out from ambient to 623 K aiming at investigating the effect of temperature on the solid solution strengthening.

2. Experimental procedures

Commercial high purity Mg ingots were melted in an electrical resistance furnace, and then pure Sn ingots with nominal composition (see Table 1) were added at 1023 K; after uniformly stirring and holding for 30 mins, the melt was poured into a mild steel mould with a diameter of 100 mm preheated at 573 K. The chemical compositions were determined by using inductively coupled plasma atomic emission spectroscopy (ICP-AES) and the analyzed results are listed in Table 1. The as-cast samples were solution treated and quenched into hot water, and the solid solution parameters are also listed in Table 1. Phase identification was determined by X-ray diffraction (XRD) (RigakuD/max 2400 X-ray diffractometer) with Cu Kα radiation.

The samples for optical microscopy were electropolished in a solution comprising 5% perchloric acid and 95% ethanol for 30–60 s at 243 K and a voltage of 15 V. Microstructural observation for backscattered electron imaging was conducted on a Philips XL30 ESEM-FEG/EDAX scanning electron microscope.

Tensile specimens were cut from the solution treated samples, and machined into dog bone shape of 5 mm gauge length and 2.4 mm × 3 mm cross-section. Tensile tests were conducted on a Sans type tensile testing machine with an initial crosshead speed of 1 mm/min, from room temperature up to 623 K. At least three tests were carried out under all test conditions. For the tests above room temperature, specimens were held for 10 min at the selected temperature, which was controlled to within ±2 K. Hardness measurement tests were performed on a Vickers tester with a load of 500 g and holding time of 15 s. No fewer than nine indents were made for each specimen.

Grain size measurements were carried out using the linear intercept method with $d = 1.74\,L$ (L is the size of the linear intercept). At least 200 grain boundaries were counted for each composition to obtain an average grain size.

3. Results and discussion

3.1. Solid solution effects on hardness

Fig. 1(a) and (b) shows the microstructures of the Mg–2.2 at.% Sn binary alloy in the as-cast and solution-treated state, respectively.

* Corresponding author. Tel.: +86 24 23926646; fax: +86 24 23894149.
E-mail address: rschen@imr.ac.cn (R.S. Chen).

0925-8388/$ – see front matter.
doi:10.1016/j.jallcom.2010.12.065

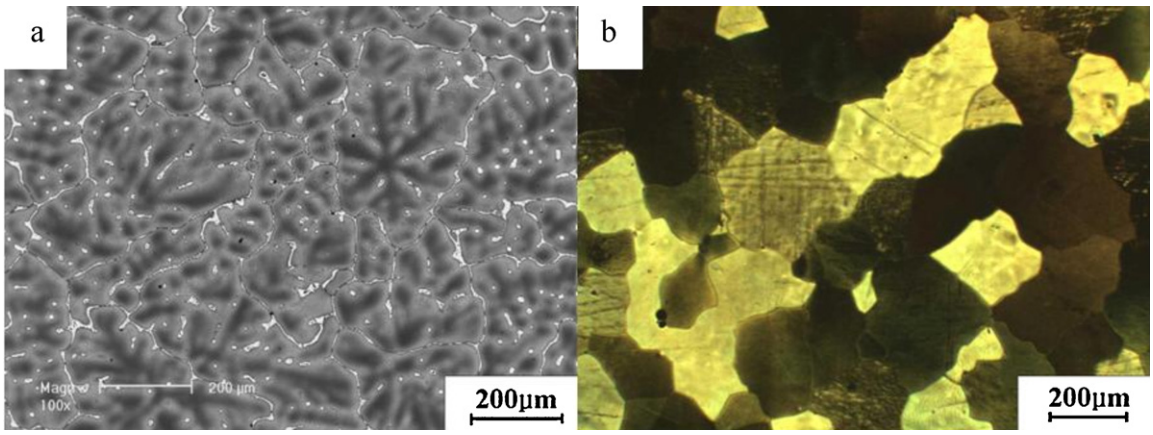

Fig. 1. Microstructure of Mg–2.2 at.% Sn alloy (a) SEM photograph in the as-cast state; (b) Optical image in the solid-solution state.

Table 1
Sn content, grain size and solution treatment conditions of the alloys in this study.

Nominal Sn content (at.%)	0.2	0.8	1.6	2.2
Analyzed Sn content (at.%) [wt.%]	0.18 [0.90]	0.75 [3.63]	1.52 [7.12]	2.18 [10.70]
Average grain size (μm)	591	409	286	291
Solution treatment	723 K/8 h	723 K/10 h	793 K/12 h	793 K/14 h

No second phases were observed after the solution treatment; this was the case for all the compositions studied after solution treatment. The average grain sizes are listed in Table 1, and decrease with increasing concentration of Sn. The XRD patterns of the solution treated alloys (in Fig. 2) indicate that all the alloys were single phase. The XRD results and microstructural observations agree with the Mg–Sn phase diagram; the solubility of Sn in magnesium is about 3.0 at.% at 793 K [4].

As shown in Fig. 3, the hardness of the experimental alloys increases monotonically with the concentration of Sn. The data for Mg–Al [10], Mg–Zn [11] and Mg–Y [12] are also included, and all the data follow a similar linear relationship. The best fit line for the Mg–Sn data points shows that the hardness ($H_{v0.5}$) is related to the Sn content (c) as

$$H_{v_{0.5}}(\mathrm{kg\,mm^{-2}}) = 28.34 + 6.88c \quad (R^2 = 0.994) \tag{1}$$

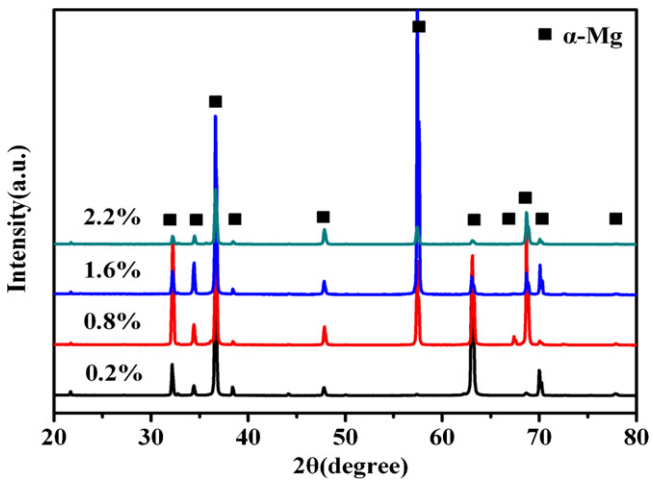

Fig. 2. XRD patterns of solution treated Mg–Sn binary alloys. The labels indicate the concentration of Sn in at.%.

Fig. 3 and Eq. (1) indicate a near linear increase of hardness with solute concentration (≈6.88 kg mm^{-2}/at.% Sn), which is dramatically higher than that reported for Mg–Al alloys (≈3.3 kg mm^{-2}/at.% Al) [10], but lower than that for Mg–Zn alloys (≈9 kg mm^{-2}/at.%Zn) [11] and Mg–Y alloys (≈13.23 kg mm^{-2}/at.% Y) [12].

3.2. Solid solution effect on the 0.2% proof strength

Representative true stress-true strain curves for the alloys are shown in Fig. 4(a), and the average values of three tensile testing results have been plotted versus the Sn concentration (see Fig. 4(b)). With increasing Sn content, the ultimate tensile strength (σ_{UTS}) and the 0.2% proof strength ($\sigma_{0.2}$) increased monotonically, while a maximum value for the elongation-to-failure (ε_f) was observed for the Mg–1.6 at.% Sn alloy.

The strengthening effects in the single phase Mg–Sn alloys originate from solid solution strengthening and grain size strengthening effect. The grain size strengthening effect, defined as $\Delta\sigma_g$, can be estimated by the Hall–Petch law [14]:

$$\Delta\sigma_g = \sigma_0 + kd^{-1/2} \tag{2}$$

where $\sigma_0 = 11\,\mathrm{MPa\,\mu m^{1/2}}$ for pure magnesium [10–12,15], k is a parameter determined for the polycrystalline material, and d is the grain size from Table 1. No detailed studies are available on the Hall–Petch laws in Mg–Sn binary alloys. The value

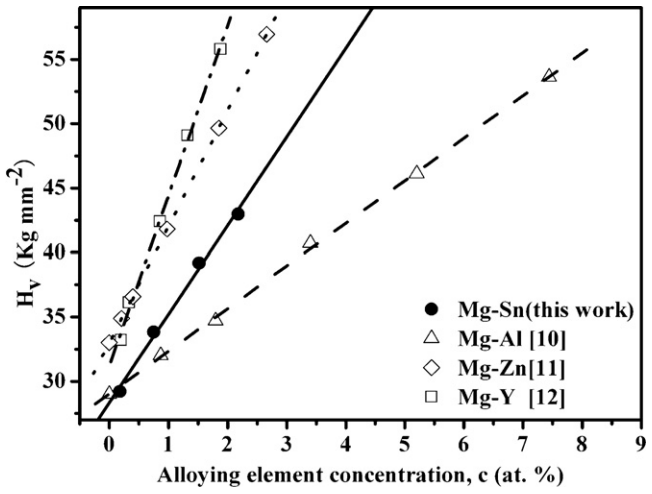

Fig. 3. The Victors hardness as a function of the concentration of alloying elements. The data of Mg–Al [10], Mg–Zn [11] and Mg–Y [12] are also included in the figure for comparison.

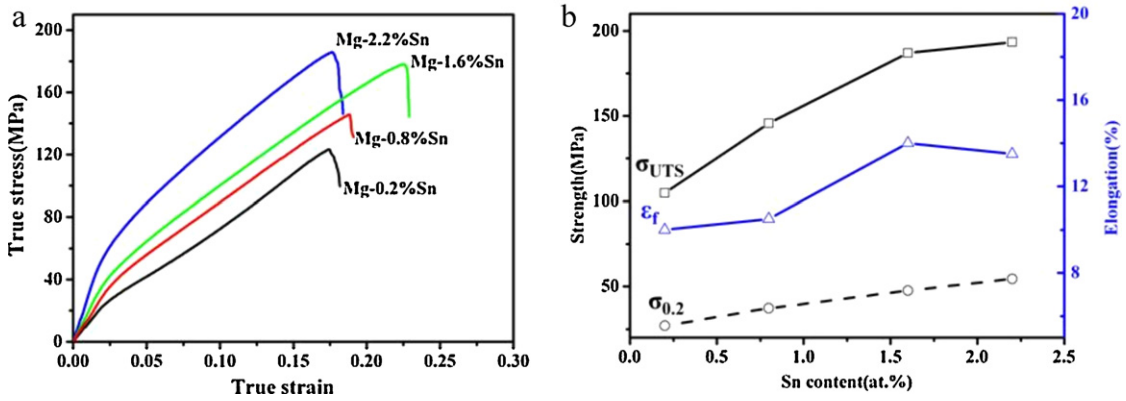

Fig. 4. (a) Tensile flow curves of Mg–Sn binary alloys at room temperature. (b) Tensile properties of the Mg–Sn alloys as a function of the atom concentration of solute. $\sigma_{0.2}$ is the 0.2% proof strength; σ_{UTS} is the ultimate tensile strength; and ε_f is the elongation-to-failure. The labels indicate the concentration of Sn in at.%.

$k = 220$ MPa $\mu m^{1/2}$ [10–12,15] in pure Mg is used for the following analysis. It is also assumed that k is independent of alloy composition. Accordingly, the effect of solid solution strengthening $\Delta\sigma_s$ can be calculated as follows:

$$\Delta\sigma_s = \sigma_{0.2} - \Delta\sigma_g = \sigma_{0.2} - (\sigma_0 + kd^{-1/2}) \quad (3)$$

where $\sigma_{0.2}$ is the 0.2% proof strength read from Fig. 4(b); $\Delta\sigma_g$ is the value for grain size strengthening effect.

The effect of solid solution strengthening $\Delta\sigma_s$ can be obtained by using the method mentioned above. Fleischer [16] and Labusch [17,18] developed different solid solution models based on the solute concentration dependence of yield strength as follows:

$$\sigma_{ys} = \sigma_{y0} + Z_F G {\xi_F}^{3/2} c^{1/2} \quad (4)$$

$$\sigma_{ys} = \sigma_{y0} + Z_L G {\xi_L}^{4/3} c^{2/3} \quad (5)$$

where σ_{y0} is the yield stress of pure magnesium; Z_L and Z_F are constants, ξ_F and ξ_L are different linear combination of the size misfit parameter and the modulus misfit parameter (the subscripts L and F stand for Labusch and Fleischer, respectively); G is the shear modulus of pure magnesium; c is the atomic concentration of solute atoms.

Since both the two equations developed by Fleischer [16] and Labusch [17,18] suggested that the solid solution strengthening effect of various solutes arises from the size misfit and modulus misfit parameters [16], the two equations should be generally applied to describe the solid solution strengthening effect in the magnesium alloys with different alloying elements. In this work the solid solution strengthening effect $\Delta\sigma_s$ of Mg–Sn alloys were plotted in Fig. 5 as a function of $c^{1/2}$ and $c^{2/3}$ ($R^2 = 0.996$ and 0.999). As observed from the solid lines in this figure, all data points follow both equations well in this composition range; which is also the case for the data of Mg–Al [10] and Mg–Y alloys [12] at all concentrations, and Mg–Zn alloys [11] at concentration above 0.7 at.%. The slopes (in MPa $(at.)^{-n}$) of the best fit lines for Mg–Sn polycrystalline alloys, are 233 and 389 for $n = 1/2$ and 2/3, respectively.

Caceres and Rovera [10] demonstrated that the strengthening of the basal plane controls the solid solution strengthening in polycrystalline Mg–Al alloys. Van Der Planken and Deruyttere [19] tested the critical resolved shear stress (CRSS) data in the monocrystalline Mg–Sn solid solutions with different levels of containing elements. Combined with relevant Schimid factors [19], the data for the CRSS of basal slip in basal planes in single crystals are obtained and also plotted in Fig. 5 as a function of $c^{1/2}$ and $c^{2/3}$ ($R^2 = 0.973$ and 0.984) for comparison.

Consequently, the evaluation of the strengthening effect arising from the basal plane in polycrystals of Mg–Sn alloys, σ_b, can be estimated as [10]:

$$\sigma_b = m\Delta\tau_s = mB_n(c - c_0)n \approx mB_n c^n \quad (6)$$

where m is the Taylor orientation factor connecting the tensile flow stress of the polycrystals to the CRSS of the relevant slip systems. It was reported by R. Armstrong et al. [20] that m corresponds to 6.5 for magnesium with a theoretical random texture, while Lukáč [21] suggested that m should lie between 4 and 6. Due to lack of relevant data, a mean value of $m = 5.5$ was adopted in this paper. B_n (in MPa $(at.)^{-n}$) is the solid solution strengthening rate on the basal plane for single crystals of Mg–Sn alloys. From Fig. 5, the values of B_n (the slopes of the dashed lines, in MPa $(at.)^{-n}$) were determined as 35 and 52 for $n = 1/2$ and 2/3, respectively. Substituting m and B_n into Eq. (6), the strengthening effect arising from the basal plane in polycrystals of Mg–Sn alloys, σ_b (in MPa $(at.)^{-n}$) was estimated as follows:

$$\sigma_b \approx 5.5B_n c^n = 192.5\left(\text{for } n = \frac{1}{2}\right) \text{ or } 286\left(\text{for } n = \frac{2}{3}\right) \quad (7)$$

So, the proportion (η) of σ_b to the solid strengthening effect in the polycrystalline Mg–Sn alloys (from the slope of the solid lines

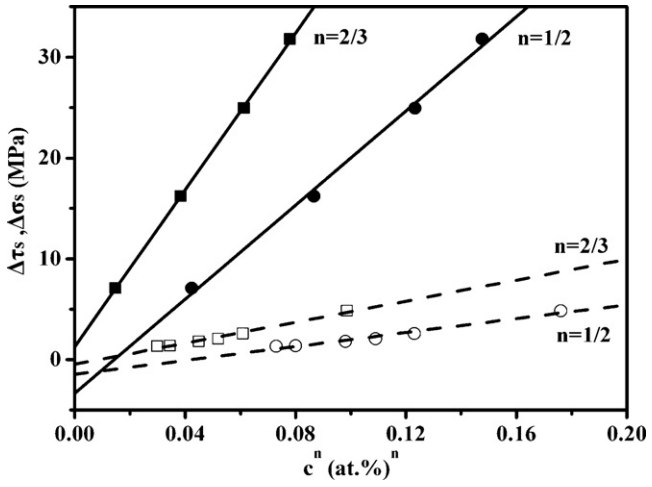

Fig. 5. The best fit lines with solid symbols (denoted as $\Delta\sigma_s$ in the vertical axis) represent the average experimental 0.2% proof strength data after subtracting the grain size strengthening effect calculated by Eq. (2); The best fit lines with open symbols (denoted as $\Delta\tau_s$ in the vertical axis) correspond to the critical resolved shear stress (CRSS) of basal slip in the basal plane in monocrystalline Mg–Sn alloys [19].

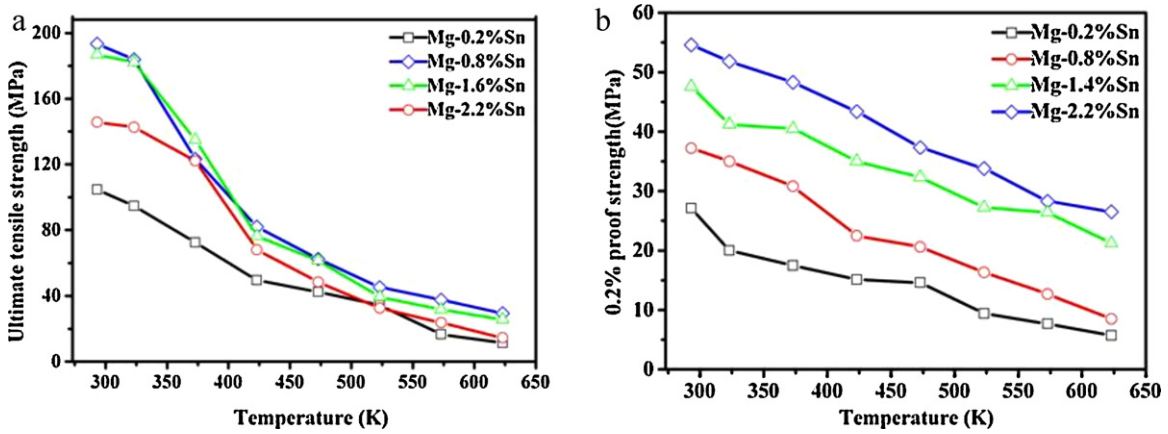

Fig. 6. Ultimate tensile strength and 0.2% proof strength ($\sigma_{0.2}$) for the studied alloys versus temperature. The labels indicate the concentration of Sn in at.%.

in Fig. 5) is:

$$\eta = \frac{192.5}{233} = 83\% \left(\text{for } n = \frac{1}{2}\right) \text{ or } 286/389 = 74\% \left(\text{for } n = \frac{2}{3}\right) \quad (8)$$

From the above calculations, it can be seen that the strengthening of the basal plane dominates the solid solution strengthening for polycrystalline single-phase Mg–Sn alloys.

Note that a common feature of both Eq. (4) and (5) is that the plots of $\Delta\sigma_s$ versus $c^{1/2}$ or $c^{2/3}$ should pass through σ_{y0} (the yield strength of pure Mg in this case). However, the values of σ_{yo} extrapolated from the fitted line (−3 MPa and 1 MPa for $c^{1/2}$ and $c^{2/3}$) are unrealistic, since the yield strength of pure Mg cannot be negative. Despite lack of strength data for the low compositions in this study, one possible explanation for this effect may be a higher strengthening rate at higher compositions. A similar phenomenon was observed in concentrated Mg–Zn alloys [11] in which the strengthening rate at concentrations above 0.7 at.% is higher than that at dilute concentrations, and the author suggest that the increased rate of strengthening in concentrated Mg–Zn alloys should be ascribed to the formation of regions of SRO (short-range ordering) during the solution heat treatment [11]. Van Der Planken and Deruyttere [19] estimated the contribution of SRO in single crystals of Mg–Sn alloys, but the calculation is very rough due to lack of relevant parameters. Accordingly the formation of SRO can also be assumed to have a strengthening effect on the concentrated alloys which accounts for a negative value by extrapolation. Although such an assumption is reasonable, the correct explanation is not certain. Further experiments are needed to verify the existence of SRO in the Mg–Sn system.

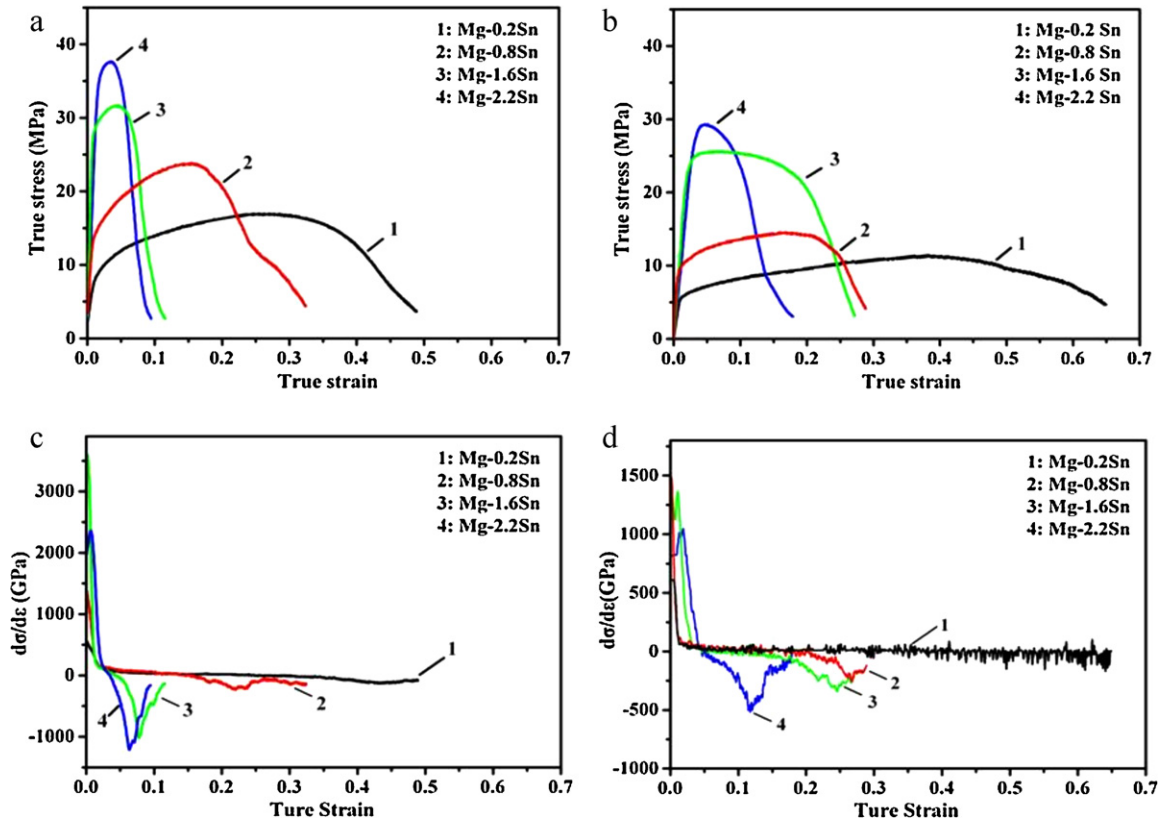

Fig. 7. Typical tensile flow curves for the studied alloys (a) at 573 K and (b) at 623 K; the strain-hardening rate versus true strain (c) at 573 K and (d) at 623 K. The labels indicate the concentration of Sn in at.%.

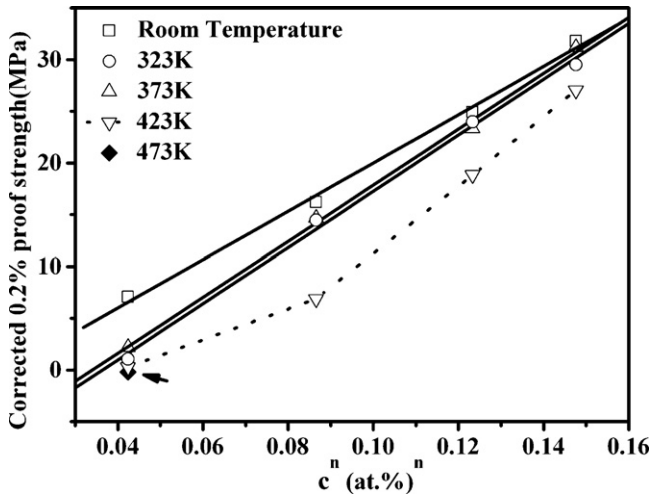

Fig. 8. 0.2% proof strength after correction from grain size strengthening effect by Eq. (3) as a function of $c^{2/3}$. The arrow points at the corrected value of 0.2% proof strength for Mg–0.2 at.% alloy at 473 K.

3.3. Temperature dependence of the 0.2% proof strength

Tensile tests were carried out in the temperature range 293–623 K. Fig. 6(a) and (b) show the change in ultimate tensile strength and 0.2% proof strength ($\sigma_{0.2}$) versus temperature for the alloys; both of them decline monotonically with increasing temperature.

Fig. 7(a), (b) shows typical tensile flow curves at 573 K and 623 K, the changes in the strain-hardening rate of the tensile curves in Fig. 7(a) and (b) versus true strain are plotted in Fig. 7(c) and (d), respectively. For the Mg–1.6 at.% Sn and Mg–2.2 at.% Sn alloy, a clear drop is observed after the yield point in the tensile flow curves at 623 K and the highest strain-hardening rate of the tensile plots at 623 K is one half of that at 573 K. One effect to be considered is the softening effect of solute atoms, which caused the decrease in yield strength seen in Fig. 6(b), and a negative strain-hardening rate with increasing temperature. It can be expected that softening effect dominates the strengthening effect at 623 K for the high compositions, while the softening effect for lower compositions manifests at lower temperatures. From the tensile plots of the Mg–0.2 at.%Sn and Mg–0.8 at.% Sn alloys, the stable plastic deformation region in which the strain-hardening rate is close to zero occurs above 573 K (see Fig. 7(c) and (d)), indicating that a dynamic equilibrium between the strengthening and softening effects occurs at this temperature. Actually the occurrence of the softening effect may also be indicated from Fig. 6(a); the difference in the UTS between different compositions is small when the temperature is above 423 K.

It was confirmed that the Hall–Petch relationship holds for polycrystalline magnesium at higher temperatures up to 523 K [15,22]. After correction from grain size strengthening effect by Eq. (3) with relevant parameters [15,22], the 0.2% proof strength was replotted as a dependence of $c^{2/3}$ in Fig. 8. The 0.2% proof strength exhibits a linear relationship with $c^{2/3}$ from room temperature to 373 K. However, the corrected 0.2% proof strength deviate from the c^n power law at 423 K; moreover, the corrected value for Mg–0.2 at.% Sn alloy is negative at 473 K (pointed by the arrow in Fig. 8). That indicates that the softening effect is expected at higher temperatures, that is, the c^n power-law is not applicable in the temperature range of 423–623 K. The data tested at temperatures higher than 473 K are not plotted in Fig. 8.

The temperature dependence of the yield stress can be explained by assuming that it is controlled by the thermally activated dislocation processes. At higher temperatures, there is a dynamic balance between the build up of dislocations, leading to strengthening, and the annihilation of dislocations, leading to softening [23]. One possible factor related to the softening effect is the decrease in the CRSS for non-basal slip systems with increasing temperature, which has been demonstrated by many authors [24,25]. Another possible factor is dynamic recovery, which has been accepted as one of the softening mechanisms in magnesium alloys during higher temperature deformation [26], especially when the temperature is above $0.4T_m$ (T_m is the melting point of the alloy). In addition, the precipitation of Mg_2Sn phase [27] and dynamic recrystallization should also be discussed. Considering that the total holding and testing time for every sample at high temperatures were not more than 15mins, no precipitation hardening can occur in such short testing time and that has been reported in the Mg–Y alloys [28]. Consequently the precipitation of Mg_2Sn phase should be ruled out. Moreover, because no recrystallized grains were observed according to the microstructure examination conducted at higher temperatures, the contribution of dynamic recrystallization should also be ignored.

In this study the fact that the c^n power-law for polycrystalline Mg–Sn binary alloys cannot apply in the temperature range 423–623 K has been explained by the competition between the solid solution strengthening effect and the softening effect. The latter may be due to the decrease in the CRSS for non-basal slip systems and the occurrence of dynamic recovery. With increasing temperature, a point is reached at which the softening effect dominates the strengthening effect. However, there may be other factors that have not been considered in this discussion, such as the contribution of SRO (short-range-ordering) [19,29–31] due to lack of correlative parameters. Further investigations are needed to understand the strengthening/softening mechanisms for Mg–Sn alloys especially at elevated temperatures.

4. Conclusions

Four compositions (0.2, 0.8, 1.6, 2.2 at.%) of polycrystalline Mg–Sn binary alloys were chosen to investigate the solid solution effect in the temperature range from ambient to 623 K. The hardness increased with the Sn content as $H_{v0.5} = 28.3 + 6.88c$.

After correcting for the grain size effects, the 0.2% proof strength of the Mg–Sn alloys follows a linear relationship with c^n, where c is the atom fraction and $n = 1/2$ or $2/3$. It is suggested that the strengthening of the basal plane controls the solid solution strengthening of polycrystalline Mg–Sn binary alloys.

The c^n power-law is not applicable in the temperature range 423–623 K, which is attributed to the opposing contributions of the solid solution effect and the softening effect. The softening effect may be caused by the decrease in the CRSS for non-basal slip systems and the occurrence of the dynamic recovery.

Acknowledgements

The author is indebted to Dr. L. Gao for some valuable suggestions, and National Basic Research Program of China (973 Program) through project no. 2007CB613704 for financial support.

References

[1] H.M. Liu, Y.G. Chen, H.F. Zhao, S.H. Wei, W. Gao, J. Alloys Compd. 504 (2010) 345–350.
[2] T.T. Sasaki, J.D. Ju, K. Hono, K.S. Shin, Scripta Mater. 61 (2009) 80–83.
[3] T.T. Sasaki, K. Oh-ishi, T. Ohkubo, K. Hono, Mater. Sci. Eng. A (2008), doi:10.1016/j.msea.2010.05.010.
[4] F.G Meng, J. Wang, L.B. Liu, Z.P. Jin, J. Alloys Compd. 508 (2010) 570–581.
[5] H.D. Zhao, G.W. Qin, Y.P. Ren, W.L. Pei, Y. Guo, J. Alloys Compd. 481 (2009) 140–143.
[6] I.-H. Jung, J. Kim, J. Alloys Compd. 494 (2010) 137–147.
[7] C. Jihua, C. Zhenhua, Y. Hongge, Z. Fuquan, J. Alloys Compd. 467 (2009) L1–L7.

[8] H. Sevik, S. Acikgoz, S.C. Kurnaz, J. Alloys Compd. 508 (2010) 110–114.
[9] B.H. Kim, S.W. Lee, Y.H. Park, I.M. Park, J. Alloys Compd. 493 (2010) 502–506.
[10] C.H. Caceres, D.M. Rovera, J. Light Met. 1 (2001) 151–156.
[11] C.H. Caceres, A. Blake, Phys. Status Solidi A 194 (2002) 147–158.
[12] L. Gao, R.S. Chen, E.H. Han, J. Alloys Compd. 472 (2009) 234–240.
[13] L. Gao, R.S. Chen, E.H. Han, J. Alloys Compd. 481 (2009) 379–384.
[14] A.H. Cottrell, An Introduction to Metallurgy, Edward Arnold, London, 1967.
[15] F.E. Hauser, P.R. Landon, J.E. Dorn, AIME Trans. 206 (1956) 589–593.
[16] R.L. Fleischer, in: D. Peckner (Ed.), Strengthening of Metals, Reinhold, New York, 1964, pp. 114–117.
[17] R. Labusch, Phys. Status Solidi A 41 (1970) 659–664.
[18] R. Labusch, Acta Metall. 20 (1972) 917–927.
[19] J. Van Der Planken, A. Deruyttere, Acta Metall. 17 (1969) 451–454.
[20] R. Armstrong, I. Codd, R.M. Douthwaite, N.J. Petch, Phil. Mag. 7 (1962) 45–58.
[21] P. Lukáč, in: G.W. Lorimer (Ed.), Third International Magnesium Conference, The Institute of Materials, London, 1997, pp. 516–524.
[22] N. Ono, R. Nowak, S. Miura, Mater. Lett. 58 (2003) 39–43.
[23] P. Lukáč, Z. Trojanová, Mater. Sci. Eng. A 462 (2007) 23–28.
[24] J.F. Stohr, J.P. Poirier, Phil. Mag. 25 (1972) 1313–1329.
[25] S. Ando, K. Nakamura, K. Takasima, H. Tonda, J. Jpn. Inst. Light Met. 42 (1992) 765–771.
[26] S.M. Zhu, J.F. Nie, Scripta Mater. 50 (2004) 51–55.
[27] S.H. Wei, Y.G. Chen, Y.B. Tang, H.M. Liu, S.F. Xiao, G. Niu, X.P. Zhang, Y.H. Zhao, Mater. Sci. Eng. A 492 (2008) 20–23.
[28] M. Sugamata, S. Hanawa, J. Kaneko, Mater. Sci. Eng. A 226–228 (1997) 861–866.
[29] R. Agarwal, H. Feufel, F. Sommer, J. Alloys Compd. 217 (1995) 59–64.
[30] S. Gorsse, C.R. Hutchinson, B. Chevalier, J.F. Nie, J. Alloys Compd. 392 (2005) 253–262.
[31] I.H. Jung, J. Kim, J. Alloys Compd. 494 (2010) 137–147.